Experimental Test of Baryon Conservation*

H. S. GURR,† W. R. KROPP,† AND F. REINES†
Case Institute of Technology, Cleveland, Ohio

AND

B. MEYER
University of the Witwatersrand, Johannesburg, Republic of South Africa

(Received 15 December 1966)

A 162-m² sr scintillation detector located 3200 m underground was used to look for high-energy fragments from baryon-nonconserving nucleon decay. A new lower limit on the half-life of the nucleon from 2×10^{28} to 8×10^{29} years, depending on the assumed decay mode, is established.

I. INTRODUCTION

THE law of baryon conservation, which asserts that in any transformation the number of baryons minus the number of antibaryons remains a constant, was first formulated as the law of conservation of nucleons by Stückelberg[1] and Wigner[2] and later evolved into its present form as the hyperons or "heavy baryons" were discovered. The law has been found valid in innumerable direct observations of reactions between particles and no violations have been reported. As is true with all physical laws, there is continued interest in testing the range of validity of baryon conservation. Some limits can be set quite simply. For example, it is reasonable that the nucleon half-life is greater than the age of the universe ($>10^{10}$ yr) and from measurements of the ambient level of radioactivity it follows for decay modes which produce such radioactivity that the half-life is greater than 10^{17} yr.

Table I summarizes the results of previous experiments which sought to detect nucleon decay. As with the present work these experiments have been able to specify only a lower limit to the half-life[3] for specific decay modes. The present work establishes more stringent limits for modes of decay which produce high-energy ionizing particles.[4–8] The effect of the nuclear binding on the half-life is assumed to be unimportant in view of the relatively small binding energy as compared with the nucleon rest mass. The results are based on measurements made in conjunction with the Case-Wits[9] neutrino experiment.

It is interesting to relate the lifetime limits to limits on the strength of baryon-nonconserving decays. If, as discussed by Feinberg and Goldhaber,[10] the matrix element M for a baryon-nonconserving two-body decay, $p\rightarrow a_1+a_2$, is taken as $M\approx B\psi_1\psi_p\Phi_2$ then the measured mean lifetime τ_p is given by $\tau_p\approx(\hbar/m_pc^2)(1/B^2)$ (sec), where $\hbar/m_pc$ is the proton Compton wavelength. A lower limit on the lifetime of 10^{29} yr therefore corresponds to $B^2\lesssim10^{-61}$.

This number can be compared with that for the strength of the gravitational interaction written in dimensionless form $G(m_p^2/\hbar c)=5\times10^{-39}$, where G is the gravitational constant. This comparison, though valid only for the interactions specified, suggests that the baryon-nonconserving interaction, if it exists, is very much weaker than the gravitational interaction.

The apparatus was a 162-m² steradian scintillation detector located 3200 m below the surface in a gold mine near Johannesburg, South Africa. The experiment differs from those which precede it primarily in the large size of the detector and the greatly reduced cosmic-ray background associated with the extreme depth of the apparatus.

II. HIGH-ENERGY DECAY-FRAGMENT METHOD

Nucleons in a given sample of material are here presumed to decay into high-energy ionizing particles in a manner which obeys all conservation laws except baryon and lepton conservation.[11] From the rate of observed events and the detector configuration we deduce the nucleon half-life or a lower limit, if the events cannot be clearly ascribed to nucleon decay.

We consider several plausible nucleon decay modes, (see Table II) consistent with the conservation of energy, momentum, spin, and charge. The limits based

* Work performed under the auspices of the U. S. Atomic Energy Commission. Based on a thesis presented by H. S. Gurr in partial fulfillment of the Ph.D. requirements at Case Institute of Technology.

† Present address: Department of Physics, University of California, Irvine, California.

[1] E. C. G. Stückelberg, Helv. Phys. Acta **11**, 225, 229 (1938).

[2] E. P. Wigner, Proc. Am. Phil. Soc. **93**, 521 (1949); Proc. Natl. Acad. Sci. (U. S.) **38**, 449 (1952).

[3] Half-lives are here used to relate the observed rate of events to the sensitivity of the detector to nucleon decay. There is no implication that the concept of time, as we know it, is valid on the scale of 10^{20} yr.

[4] F. Reines, C. L. Cowan, Jr., and M. Goldhaber, Phys. Rev. **96**, 1157 (1954).

[5] F. Reines, C. L. Cowan, Jr., and H. W. Kruse, Phys. Rev. **109**, 609 (1957).

[6] G. K. Backenstoss, H. Frauenfelder, B. D. Hyams, L. J. Koester, Jr., and P. C. Marin, Nuovo Cimento **16**, 749 (1960).

[7] C. C. Giamati and F. Reines, Phys. Rev. **126**, 2178 (1962).

[8] W. R. Kropp and F. Reines, Phys. Rev. **137**, 740 (1965).

[9] Case Institute of Technology, Cleveland, Ohio; University of the Witwatersrand, Johannesburg, Republic of South Africa.

[10] G. Feinberg and M. Goldhaber, Proc. Natl. Acad. Sci. (U. S.) **45**, 1301 (1959). See also R. E. Marshak and E. C. G. Sudarshan, *Introduction to Elementary Particle Physics* (Interscience Publishers, Inc., New York, 1961), Chap. 4.

[11] The decay of the nucleon to known particles is not possible if *only* the baryon conservation constraint is relaxed.

TABLE I. Summary of nucleon half-life experiments.

Experimenters	Nucleon half-life (yr)	Nucleon decay detection method	Nucleon source
Goldhaber (1954) (private communication)	$>1.4\times10^{18}$	Spontaneous fission of Th^{232} after excitation by nucleon decay. Assumes that the rearrangement energy upon loss of a nucleon is sufficient to cause fission of the residual nucleus.	
Reines, Cowan, and Goldhaber (1954) (Ref. 4)	$>1\times10^{22}$	High-energy decay fragment. Liquid scintillation, 30 m below surface.	Toluene in detector and surrounding paraffin.
Reines, Cowan, and Kruse (1957) (Ref. 5)	$>4\times10^{23}$	Proton decay in deuteron. High-energy fragment plus neutron left over from deuteron after decay of proton. Delayed coincidence and liquid scintillation, 61 m below surface.	
Backenstoss, Frauenfelder, Hyams, Koester, and Marin (1960) (Ref. 6)	$>2.8\times10^{26}$	High-energy fragment; upward going particles. Čerenkov and scintillation, 800 m below surface. At least 250 MeV assumed to be available to decay particle. Result based on combined measurements for neutrons and protons.	Water, lead, and rock.
Giamati and Reines (1962) (Ref. 7)	$>1\times10^{26}$ to $>7\times10^{27}$, depending on mode.	High-energy fragment. Liquid scintillation with anticoincidence shield, 585 m below surface.	Decalin in detector and surrounding iron.
Kropp and Reines (1964) (Ref. 8)	$>6\times10^{27}$ to $>4\times10^{28}$, depending on mode.	High-energy fragment. Liquid scintillation with anticoincidence shield, 585 m below surface.	Decalin in detector and surrounding iron.
Dix and Reines (private communication)	In progress.	Neutron left over from deuteron after decay of proton. Not dependent on decay mode.	Heavy water in detector.
Present experiment	$>2\times10^{28}$ to $>8\times10^{29}$, depending on mode.	High-energy fragment. Liquid scintillation, 3200 m below surface. Horizontally going particles.	Surrounding rock, mineral oil scintillator, and detector box.

on these modes are representative of those which could be established for other decay modes involving ionizing particles. It is recognized that the charged particle or particles from events of very high-particle multiplicity might not have sufficient energy to be detected. The particle energies listed follow from the application of energy and momentum conservation to the decay of a free nucleon. In the case of an initially bound nucleon, the residual nucleus can recoil with ~10–20 MeV but this small correction is ignored and the energies listed in the Table are assumed to apply to all nucleons.

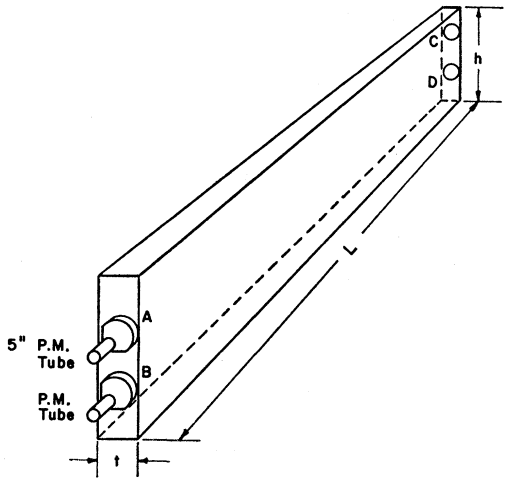

FIG. 1. Sketch of detector element. P.M. = photomultiplier.

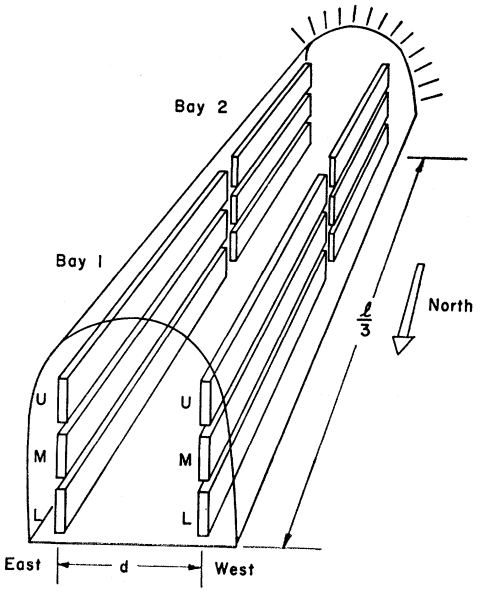

FIG. 2. Schematic of detector array showing two out of six bays.

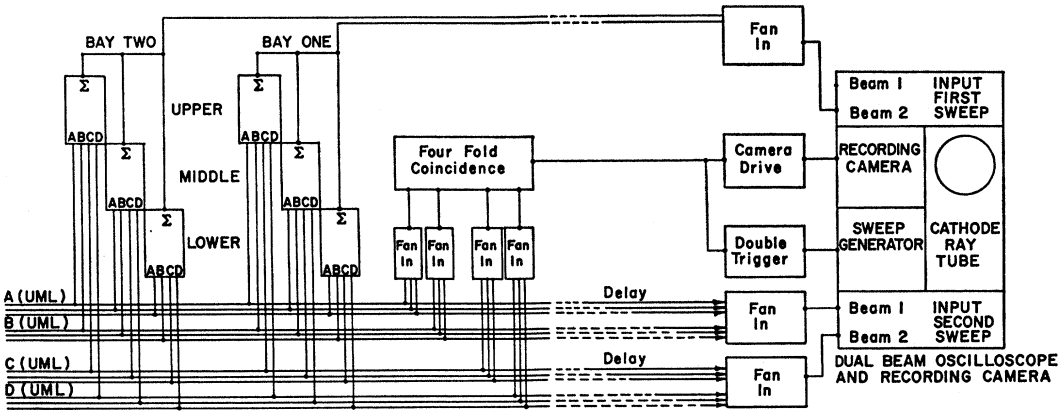

FIG. 3. Detector electronics schematic diagram for two bays on one side of array showing the groupings of photomultiplier signals into "upper," "middle," "lower," and "bay" signals, coincidence logic, and oscilloscope display. More details can be found in Ref. 12 (scintillation counter symposium).

III. EXPERIMENTAL ARRANGEMENT

The experimental arrangement is that of a detector in an underground cavity: The nucleons whose decay is sought are in the detector and the cavity walls. The wall nucleons which are sources of observable decay fragments are those within a shell having a thickness equal to the range of the decay particles.

Equation (1) relates the nucleon half-life to experimental quantities.

$$T_{1/2}=(\ln 2)\frac{N_{\text{eff}}}{\Delta N/\Delta t}, \tag{1}$$

$T_{1/2}$ = nucleon half-life,

$N_{\text{eff}}=n_d V_{\text{eff}}+n_w R_w A_{\text{eff}}$ = effective number of nucleons,

where $\Delta N/\Delta t$ = nucleon decay event rate, R_w = range of decay fragment, n_d = number of nucleons per unit volume in detector, n_w = number of nucleons per unit volume in walls of cavity, A_{eff} = effective area of detector = shadow area of detector averaged over all angles, and V_{eff} = effective volume of detector = detector volume within which decay is detected with 100% efficiency.

This equation embodies the result that the response of a detector to two-body nucleon decay fragments in a cavity with thick homogeneous walls is independent of the cavity shape or size.

IV. DESCRIPTION AND OPERATION OF THE DETECTOR

Since the detector has been described elsewhere,[12,13] only a brief description will be given here. It is an array of 54 liquid scintillation detector elements, each (Fig. 1) consisting of a long clear Lucite plastic box filled with a mineral-oil-based scintillator and viewed on each end by two 5-in. photomultiplier tubes. The detector elements (Fig. 2) were arranged end to end in six discontinuous rails, three rails on each side of a long horizontal tunnel. The geometry of the array was chosen to provide the largest possible area and a crude angular resolution for the detection of particles penetrating at angles greater than 45 deg to the zenith. The thickness of the detector elements was chosen so that a penetrating charged particle would deposit at least 20 MeV. Separate and identical electronic recording systems were provided for both sides of the detector array.

The electronic recording system operated in the following manner. A particle depositing energy in a single detector element would cause an output pulse from each of the four photomultiplier tubes of that detector. These pulses were passed through a coding system to a fourfold coincidence circuit and to an oscilloscope recording camera (Fig. 3). The fourfold coincidence triggering threshold was set so that any ionizing particle depositing $\gtrsim$10 MeV in any detector element would trigger both east and west recording systems. The photographic record (Fig. 4) included the following data: the designation of the element or elements in which sufficient energy had been deposited, the pulse height and pulse shape produced by each photomultiplier tube, and the relative timing of each

TABLE II. Assumed two-body modes of nucleon decay.

Nucleon	Fragment 1	Kinetic energy (MeV)	Fragment 2	Kinetic energy (MeV)
p	π^+	340	ν	458
p	K^+	105	ν	339
p	e^+	469	γ	469
p	μ^+	369	γ	464
n	π^+	340	e^-	458
n	μ^+	239	K^-	100

[12] F. Reines, M. F. Crouch, H. S. Gurr, T. L. Jenkins, W. R. Kropp, G. R. Smith, B. S. Meyer, and J. P. F. Sellschop, Phys. Rev. Letters 15, 429 (1965); see also the papers by members of the Case-Wits Group at the Scintillation Symposium, Washington, D. C., 1966 (unpublished).

[13] Proceedings of the International Conference on Weak Interactions, 1965, Argonne National Laboratory Report No. ANL-7130, 1966 (unpublished).

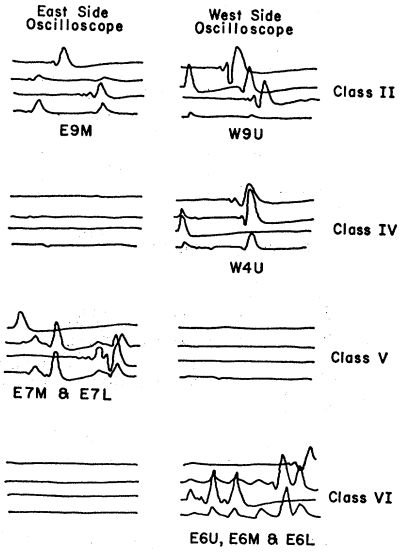

FIG. 4. Typical oscilloscope records of events involving Classes II, IV, V, and VI. Detector elements in which more than 10 MeV was deposited are designated by side (east or west), bay number, and position on given side (upper, middle, or lower).

pulse to within ± 0.2 μsec. Pulses from each side of the detector, east and west, were recorded separately and were analysed to determine the position of the event along the length of the detector as well as the energy deposited.[14] Energy resolution was estimated to be $\sim \pm 20$ percent. The desire to obtain the largest area for the available resources precluded measures to improve energy resolution.

An individual scintillation detector, identical to those below ground, was located on the surface. In this detector pulses from a radioactive gamma ray source were compared with those from penetrating cosmic ray muons. The source was then used as a secondary standard to calibrate each of the detectors below ground. The energies assigned to observed events by this calibration scheme are consistent with the energies expected from minimum-ionizing particles.

The system was regularly tested with an automatic sequencing light pulser.[15] A light pulse, very similar to that from an actual scintillation, was directed into each detector element, and the resulting electrical pulses were recorded by the cameras in exactly the same manner as an event.

The energy threshold of the system was so set that natural radioactivity which deposited energy immediately in front of the phototubes could accidently meet the fourfold coincidence requirement and regularly trigger the recording system. These background pulses provided an additional check on the sensitivity of the system but were readily distinguished from penetrating particles either because the four pulses did not originate in the same tank, or were out of time (>0.2 μsec) relative to each other.

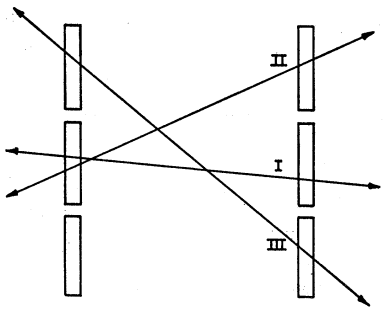

FIG. 5. End view of rail elements showing events in Classes I, II, and III.

[14] In a few cases, where elements in more than one bay on one side of the array were penetrated, the coding system did not permit an unambiguous determination of all pulse heights.

V. OBSERVED EVENTS

The features of the observed events are here compared with those expected from the modes of nucleon decay listed in Table II. Table III lists the deposited energy, position, and angle of penetration of the observed events which involve only one detector element on each side of the detector array. These cross tunnel events are divided into three classes: horizontal, e.g., U, U (Class I); intermediate, e.g., U, M (Class II); and extreme, e.g., U, L (Class III). Figure 5 shows examples of events in Classes I, II, and III. Table IV lists the number of events which involve one (Class IV), two (Class V) and three (Class VI) detector elements on one side of the detector array.

TABLE III. Events involving two detector elements, one on each side of the detector array. Period of observation, 17 months.

Class	Angle to detector normal (ξ) (deg)	Mean distance from north end of detector (m)	Energy deposited (MeV) East	West
I	+20	20.5	29	18
II	+70	26.5	55	118
I	−45	19	19	16
I	−35	6	23	24
I	−70	6	18	18
II	+20	19	5	18
II	+40	13	21	30
I	∼−40	∼20.5	∼40	25
I	+5	19.5	38	23
I	−15	27.5	20	20
II	−65	51	21	13
I	−40	46	18	18

A. Time and Position

If nucleon decay events occur, they should be at random times and be distributed uniformly throughout the detector. The observed events are consistent with these two criteria but it is recognized that the statistics are meager.

[15] For details see H. S. Gurr, Ph.D. thesis, Case Institute of Technology, 1966 (unpublished).

B. Deposited Energy (Particle Penetrating One Tank on Each Side of Detector Array)

Since the detectors are thin compared to the range of the postulated nucleon decay fragments (an exception being the kaon), they are in most cases able to measure only the ionization of the decay fragment somewhere along its range and not the total energy of the fragment. Thus the observed particles may have an energy greater than the observed deposited energy, which on the average, totals about 50 MeV. The observed energies are consistent with nucleon decay, but it is not possible to distinguish nucleon decay events from those in which other higher-energy ionizing particles may also be present (e.g., neutrino-induced muons). Events with deposited energy greater than 110-MeV total are not consistent with proton to kaon decay. All other events are taken to be consistent with nucleon decay.

C. Angle of Penetration

Nucleon decay would give rise to products which, on the average, would be isotropically distributed about the point of decay. It follows that the flux of fragments within the cavity is homogeneous and isotropic, and that the rate of detection of such fragments by a pair of detectors is proportional to the aperture of the pair.[16] Accordingly, if the observed events arise entirely from nucleon decay the intensity, which is the ratio of the rate of observed events to the aperture, should be the same for all pairs of detectors.

To facilitate a test against this criterion, the detector elements are grouped into the pairs of discontinuous rails. Identical pairs which define the same angular range are grouped into the classes shown in this figure. Table V lists the rate of observed events, aperture, and intensity for each class. The intensity for the more nearly horizontal Class I is slightly greater than that for Class II and III, as expected from neutrinos, but the data to date are statistically uncertain and the distribution is consistent with isotropy.

TABLE IV. Number of events involving elements on one side of the detector array. Period of observation, 17 months.

Class	Number of events
IV	119
V	30
VI[a]	3

[a] Class VI events are restricted to those in which the deposited energy in each detector element is >20 MeV.

[16] The aperture for a pair of detectors is the solid angle subtended by one detector at an element of area of the other detector integrated over all the elements of area. See Appendix III for an exact formulation and solution of the integral.

TABLE V. Observed events consistent with nucleon decay compared to aperture run-time product. Period of observation, 17 months.

Class	Aperture bays 1 to 6 (cm^2 sr)	Aperture bays 7 to 9 (cm^2 sr)	Total aperture ×run time (cm^2 sr/sec)	Number of events	Intensity (cm^{-2} sr^{-1} sec^{-1})
I	47.6×10^4	18.5×10^4	130×10^{11}	8	0.61×10^{-12}
II	52.2	20.2	143	4	0.28
III	17.0	6.5	46	0	0.22[a]

[a] The number of events is taken as one in estimating half-life limits.

VI. CALCULATION OF NUCLEON HALF-LIFE LIMITS

Since no feature of the observed events clearly indicates the presence of nucleon decay, only a lower limit on the nucleon half-life can be obtained from the present experiment. The lower half-life limit for each decay mode listed in Table II is calculated in two different ways and the results are given in Table VI. The half-life for each mode is calculated on the assumption that all of the events, not attributable to other causes and consistent with the mode, are due to nucleon decay in that mode alone. Calculations were based on Eq. (14) of Appendix II.

A. Nucleon Half-Life Consistent with Events in Class III (Background Not Subtracted)

It is seen from Table V that the number of events per unit aperture is lowest in Class III. The null rate in this class was arbitrarily taken to be one event during the period of observation. Half-lives calculated on this basis are shown in Table VI under the headings "Class III events only."

B. Nucleon Half-Life Consistent with Events in Classes I, II, and III (Neutrino-Induced Muon Background Subtracted)

Almost all of the events in Classes I and II can be attributed to muon-neutrino interactions in the rock

TABLE VI. Lower limits on nucleon half-lives for specified decay modes. Units of 10^{28} yr.

Assumed decay mode	Free protons: Class III events only	Free protons: Neutrino-induced background subtracted class I, II, & III	All nucleons: Class III events only	All nucleons: Neutrino-induced background subtracted class I, II, & III
$p\to\pi^+ + \nu$	0.8	1.2	9	17
$\to K^+ + \nu$	0.3	0.6	1	2
$\to e^+ + \gamma$	0.9	1.3	16	30
$\to \mu^+ + \gamma$	0.9	1.3	49	82
$n\to\pi^+ + e^-$	...	...	21	36
$\mu^+ + K^-$	...	...	25	49

surrounding the detector. Statistical considerations aside, it is predicted[17] that no fewer than eight of the twelve events listed in Table III are due to neutrinos. It would thus seem reasonable that no more than four of the events in Table III are due to nucleon decay yielding the results listed in Table VI.

VII. CONCLUSIONS AND SUGGESTIONS FOR AN IMPROVED EXPERIMENT

The data give no evidence for the existence of nucleon decay. Lower limits on the half-life of the nucleon from 2×10^{28} to 8×10^{29} yr depending on the assumed decay mode are established. It is seen that the atmospheric muon neutrino serves as the major source of background in the present experiment. If it were possible to positively identify all muon neutrino events, improved half-life limits could be established. Since the energies of nucleon decays are much lower than those from neutrino events it is possible in principle to make such an identification using absorbers between the two sides of the tunnel.

ACKNOWLEDGMENTS

We wish to thank the members of the Case-Wits Neutrino Group, especially Dr. M. F. Crouch, Dr. T. L. Jenkins, Dr. J. P. F. Sellschop, H. Sobel, A. A. Hruschka, and B. M. Shoffner, for their vital contributions to the experiment. The financial support of the U. S. Atomic Energy Commission, the hospitality of the Directors of the East Rand Proprietary Mine, and the willing assistance of the mine staff are gratefully acknowledged.

APPENDIX I. NUCLEON-DECAY COUNTING RATE IN A THIN FLAT DETECTOR

In this appendix the detector is assumed to be so thin that the fraction of particles cutting corners is negligible. In the final results (Appendix III) a correction for corner cutting is included. It is also assumed that (1) the materials of the cavity walls (rock), the active detector material (scintillator), and the detector covers (lucite, press-wood and sheet steel) were homogeneous; (2) the decay products are emitted isotropically, on the average.

A. Nucleons decaying in the Detector (One Ionizing Decay Fragment)

To discriminate against natural radioactivity a minimum detection threshold $E_T\simeq10$ MeV was selected. Since nucleon decay fragments near their origin are minimum ionizing, the path length m to deposit the threshold energy E_T is

$$m=\frac{E_T}{(dE/dx)},$$

where dE/dx is the rate of energy loss with distance in the detector. An ionizing fragment leaving a thin detector at an angle α to the detector normal and originating a distance greater than $m\cos\alpha$ from the detector edge will be counted. For a thin slab the rate at which single ionizing decay fragments emitted at angle α within solid angle $d\Omega$ are detected is

$$d^2\left(\frac{\Delta N}{\Delta t}\right)=\frac{dn_d}{dt}A\,(t+s-m\cos\alpha)\frac{d\Omega}{4\pi}, \tag{2}$$

where n_d = number of nucleons per unit volume in the detector, $(dn_d/d\tau)=(n_d/\tau)$ = nucleon decay rate per unit volume in the detector, τ = nucleon mean life, A = area of detector, t = thickness of active detector material (scintillator), $s=(\sum_i P_i x_i/P_d)$ = effective thickness of detector walls (plastic tank walls plus cover),[18] P_i = density of various materials in detector walls, x_i = thickness of various detector walls, and P_d = density of active detector material. The single ionizing decay fragment counting rate from decays in the detector is therefore

$$\frac{\Delta N}{\Delta t}=\frac{n_d}{\tau_1}\int_\Omega\frac{A\cos\alpha}{4\pi}\left(\frac{t+s}{\cos\alpha}-m\right)d\Omega=\frac{n_d}{\tau_1}V_{\text{eff}}. \tag{3}$$

B. Nucleons in the Detector (Two Ionizing Decay Fragments)

If two ionizing fragments are emitted, at least one of the fragments will be detected because the fragments proceed in opposite directions. The two-ionizing-fragment counting rate for decays in the detector volume V_d is therefore

$$\frac{\Delta N}{\Delta t}=\frac{n_d}{\tau_2}V_d. \tag{4}$$

C. Nucleons Outside the Detector (Single Ionizing Decay Fragment)

As seen from Fig. 6 the nucleon decay detection rate for a single ionizing fragment emitted from volume dV toward area dA is

$$d^5\left(\frac{\Delta N}{\Delta t}\right)=\frac{dA\cos\alpha}{4\pi r^2}\frac{dn_w}{dt}dV, \tag{5}$$

where n_w = number of nucleons per unit volume in cavity wall, r = distance from dA to dV, r_0 = distance from dA to cavity wall, $(dn_w/dt)=(n_w/\tau_1)$ = nucleon

[17] R. M. Sternheimer, in *Methods of Experimental Physics*, edited by L. C. L. Yuan and C. S. Wu, (Academic Press Inc., New York, 1961), Vol. 5, Part A, Chap. 1, p. 4.

[18] Since the plastic tank is similar in composition to the scintillator it is most easily included as part of the scintillation volume. Other parts of the detector cover are negligible but for completeness their effect is lumped into the detector wall thickness.

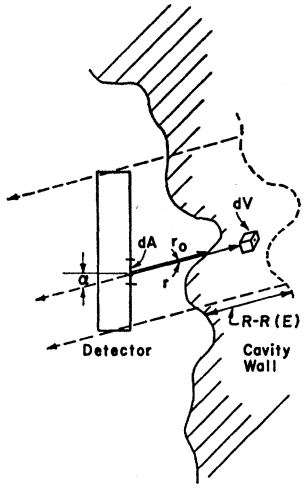

FIG. 6. Nucleon decay fragments at angle $(\alpha\beta)$ originating in volume dV and passing through dA.

decay rate per unit volume of wall, and R_w= total range of decay fragment in wall.

Since a particle is more heavily ionizing at the end of its range, a particle need have only a negligible fraction of its residual range within the detector to deposit the required threshold energy. Thus to a very good approximation the effective volume extends into the wall *along* r to a depth equal to the range of the decay fragment. The counting rate due to single ionizing fragment nucleon decay in the wall is therefore

$$\frac{\Delta N}{\Delta t}=\frac{n_w}{\tau_1}\int_A\int_\Omega\int_{r_0}^{r_0+R_w}\left(\frac{dA\cos\alpha}{4\pi}\right)d\Omega dr. \quad (6)$$

Since in the present experiment, the detector is in a cavity of wall thickness greater than R_w the result does not depend on the distance r_0 from the cavity wall to any detector element and in general,

$$\frac{\Delta N}{\Delta t}=\frac{R_w n_w}{\tau_1}\int_\Omega\left(\frac{A\cos\alpha}{4\pi}\right)d\Omega=\frac{R_w n_w}{\tau_1}A_{\text{eff}}. \quad (7)$$

D. Nucleon Decaying Outside Detector (Two Ionizing Decay Fragments)

In this case the two decay fragments proceed in opposite directions so that the counting rate is the sum of *two* terms of the form given by Eq. (7).

E. Summary

The mean lives τ_1 for single ionizing fragment nucleon decay and τ_2 two-ionizing-fragment nucleon decay are, respectively,

$$\tau_1=\frac{1}{\Delta N/\Delta t}(n_d V_{\text{eff}}+n_w R_w A_{\text{eff}}), \quad (8)$$

$$\tau_2=\frac{1}{\Delta N/\Delta t}(n_d V_d+n_w R_w' A_{\text{eff}}+n_w R_w'' A_{\text{eff}}). \quad (9)$$

APPENDIX II. NUCLEON DECAY COINCIDENCE COUNTING RATE IN TWO THIN FLAT PARALLEL DETECTORS

A. Single Ionizing Decay Fragment (τ_1)

Equations (3) and (7) of Appendix I give the coincidence rate for a single-ionizing fragment which passes through two detectors across the tunnel from each other if the area, A, is replaced by $A(\alpha,\beta)$, the area of the detector or of the cavity wall within which a nucleon decay fragment in direction (α,β), within solid angle $d\Omega$, will pass through both detectors. (See Fig. 7 for a definition of α and β.) This is the area of overlap or "shadow area" of the two detectors in the direction (α,β). The effective volumes extend *along* r into the rock a distance equal to $[R_w-R(E)_w]$ where E is the energy necessary to penetrate the first detector and reach the second. In this case Eqs. (3) and (7) become

$$\frac{\Delta N}{\Delta t}=\frac{n_d}{\tau_1}\int_\Omega\frac{A(\alpha,\beta)\cos\alpha}{4\pi}[(t+s)/\cos\alpha-m]d\Omega, \quad (10)$$

$$\frac{\Delta N}{\Delta t}=\frac{n_w}{\tau_1}\int_\Omega\frac{A(\alpha,\beta)\cos\alpha[R_w-R(E)_w]}{4\pi}d\Omega, \quad (11)$$

where $A(\alpha,\beta)$ = area of shadow on one detector cast by parallel rays in the direction (α,β) from the other detector, R_w = total range of decay fragment in rock (cm), $R(E)_w$ = range of decay fragment of energy E in rock (cm), and E = energy necessary for a fragment traveling in direction (α,β) to penetrate the first detector and just reach the active region of the second.

At those angles $\alpha\leq\alpha_0$ where $[R_w-R(E)_w]\leq 0$, the integrand in Eq. (11) is zero. At $\alpha=\alpha_0$, the function $(t+s)/\cos\alpha-m$ in Eq. (10) changes to R_d (range of the fragment in the detector).[19] The integrands may be

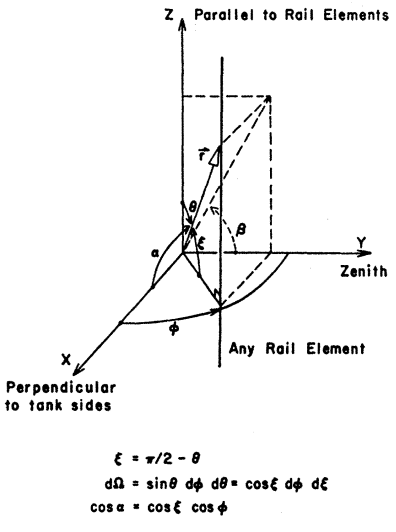

FIG. 7. Orientation coordinate system.

[19] Since in most cases $R_d\gg(t+3s)$ it is sufficiently accurate to terminate the integration in Eqs. (10) and (11) at $\alpha=\alpha_0$.

TABLE VII. Nucleon decay fragment ranges.[a]

Material	Fragment	Energy (MeV)	Range $R\rho$ (g/cm²)	Neutrons per unit area (10^{25}/cm²)	All protons per unit area (10^{25}/cm²)	Free protons per unit area (10^{25}/cm²)
SiO_2	$\pi^{\pm}$	340	168	5.07	5.07	0
	$\mu^{\pm}$	369	192	5.79	5.79	0
	$\mu^{\pm}$	239	116	3.50	3.50	0
	$e^{\pm}$	458	59.6	1.78	1.78	0
	$\gamma \rightarrow e^{\pm}$	232	45	1.35	1.35	0
$CH_{1.8}$	$\pi^{\pm}$	340	137	3.59	4.66	1.08
	$K^{\pm}$	106	12.9	0.338	0.438	0.101
	$K^{\pm}$	100	11.8	0.310	0.403	0.093
	$\mu^{\pm}$	369	157	4.11	5.34	1.25
	$\mu^{\pm}$	239	94.7	2.48	3.21	0.74
	$e^{\pm}$	458	52.8	1.58	1.78	0.20
	$\gamma \rightarrow e^{\pm}$	232	37.0	1.11	1.26	0.15

[a] Computed using techniques described by Sternheimer (Ref. 17).

considered to be valid for all angles if the roles of the two detectors are reversed when α is $>\pi/2$. Equation (11) can be simplified by noting that the range of an ionizing particle is approximately inversely proportional to the density of the stopping medium. Particle ranges are summarized in Table VII. Therefore,

$$n_w R(E)_w \simeq k n_d R(E)_d = k n_d \frac{(3s+t)}{\cos\alpha}, \quad (12)$$

where $K \approx 1$. Equation (11) becomes

$$\frac{\Delta N}{\Delta t} = \frac{1}{\tau_1} \int_{\Omega;\,\alpha<\alpha_0} \frac{A(\alpha,\beta)\cos\alpha}{4\pi} \times \left(n_w R_w - \frac{k n_d (t+3s)}{\cos\alpha} \right) d\Omega. \quad (13)$$

Adding (10) to (13) and rearranging, the total counting rate from nucleons inside and outside the detector is

$$\frac{\Delta N}{\Delta t} = \frac{(n_w R_w - m n_d)}{4\pi\tau_1} A_p - \frac{[n_d(t+s)(k-1)+2k n_d s]}{4\pi\tau_1} B_p, \quad (14)$$

where

$$A_p = \int_{\Omega;\,\alpha<\alpha_0} A(\alpha,\beta)\cos\alpha d\Omega = \text{aperture}, \quad (15)$$

$$B_p = \int_{\Omega;\,\alpha<\alpha_0} A(\alpha,\beta) d\Omega = \text{"pseudo-aperture."} \quad (16)$$

B. Two Ionizing Fragments (τ_2)

For nucleons inside the detector the decay fragments emitted in direction (α,β) and depositing energy greater than the threshold energy may originate anywhere *along r* within either detector. Hence the counting rate for nucleons inside and outside the detector is given by the sum of two terms (one for each fragment) identical to Eq. (14) with $m=0$. Each integral can without significant error in most cases be terminated at the angle α at which one of the fragments is unable to penetrate the full depth of one detector. An approximate formula for τ_2 is

$$\tau_2 = \frac{1}{(\Delta N/\Delta t)} \frac{(R_w' + R_w'') n_w}{4\pi} A_p. \quad (17)$$

APPENDIX III. COINCIDENCE APERTURE FOR LONG, NARROW, THIN, FLAT, DISCONTINUOUS, PARALLEL DETECTORS

In this Appendix the aperture A_p is particularized to the case of coincidences between two sides of an array

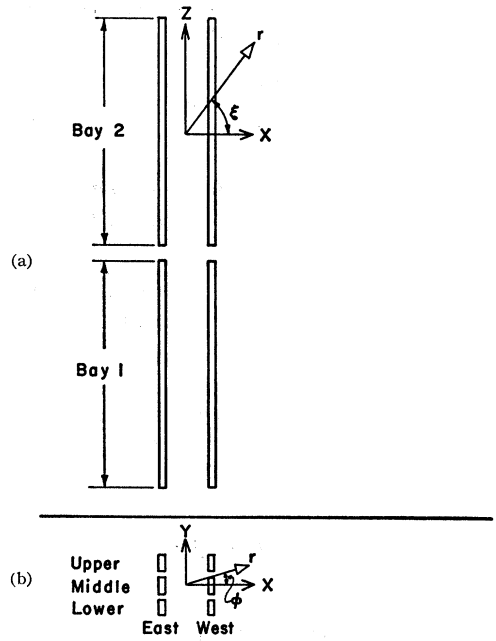

FIG. 8. (a) Top view of detector array showing first two bays. (b) End view of array.

of long parallel detectors. The calculation of the "pseudo-aperture" B_p follows almost the same steps and will not be given here. The apertures are most easily calculated using the polar coordinates (ϕ,ξ), shown in Figs. 7 and 8. In this coordinate system the aperture is[20]

$$A_p=\int_{\phi=0}^{2\pi}\int_{\xi=-\pi/2}^{\pi/2} A(\phi,\xi)(\cos\xi\cos\phi)\cos\xi d\xi d\phi, \quad (18)$$

where $A(\phi,\xi)$ vanishes for angles corresponding to directions in which it is not possible to pass a particle through the sensitive regions of both sides of the array.

The configuration is symmetric about the three mutually perpendicular planes defined by $\phi=0$, $\phi=\pi/2$, and $\xi=0$. Hence

$$A_p=8\int_{\phi=0}^{\pi/2}\int_{\xi=0}^{\pi/2} A(\phi,\xi)(\cos^2\xi\cos\phi)d\xi d\phi. \quad (19)$$

For flat parallel rectangular detectors $A(\phi,\xi)$ is the product of the length and the height of the rectangular "shadow area"

$$A(\phi,\xi)=H(\phi,\xi)L(\phi,\xi). \quad (20)$$

The boundaries of the shadow area are given by the envelope of parallel rays having path lengths in each detector greater than the threshold path length m as defined in Appendix I. A tedious but fairly straightforward consideration[15] of the geometry yields the results summarized below.

APPENDIX IV. SUMMARY

The apertures for the individual pairs of discontinuous rail detectors have been calculated following this ap-

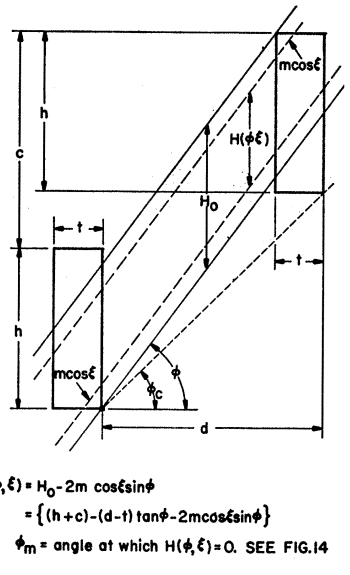

FIG. 9. Shadow height of two parallel flat detectors for angles $\phi_c<\phi<\phi_m$. End view of rail elements.

[20] In the following discussion the integrals are all terminated at ngles ξ_0 and ϕ_0 which are equivalent to α_0.

TABLE VIII. Dimensions of detector array.

Symbol	Bays 1 to 6 (cm)	Bays 7 to 9 (cm)	Definition
l	3577	1686	Total length of rail including gaps
g	59	133	Length between sensitive regions of detectors in given rail
i	14.3	14.3	Height between sensitive regions of detector elements
v	547	473	Length of detector element sensitive region
h	56	56	Height of detector element sensitive region
t	12.7	12.7	Thickness of detector element of sensitive region
s	1.6	1.6	Effective thickness of detector walls
d	180	180	Horizontal distance, center to center, between sides of detector
Q	6	3	Number of bays

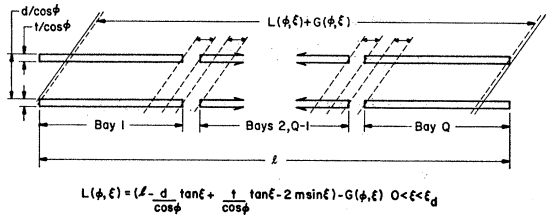

FIG. 10. Shadow length of two parallel flat discontinuous rail detectors for $0<\xi<\xi_d$. Top view of detector elements.

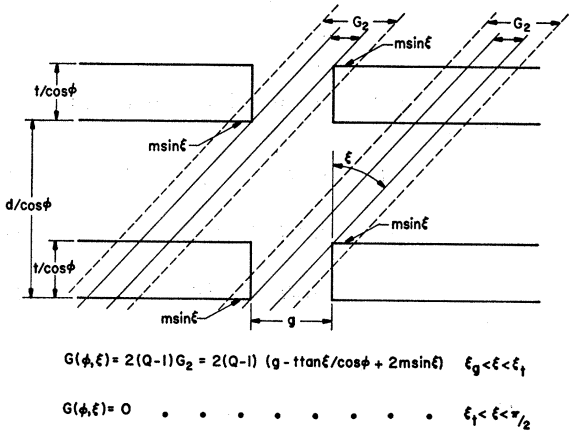

FIG. 11. Length of gaps for $\xi_g<\xi<\pi/2$. Top view of detector elements.

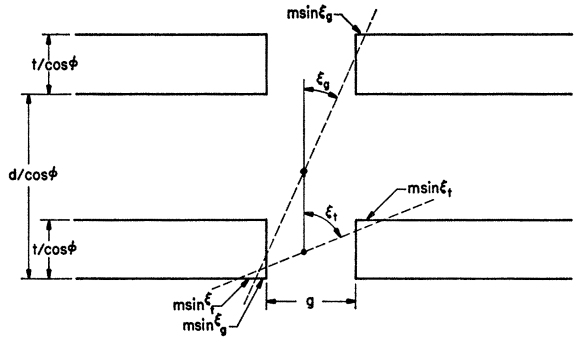

FIG. 12. Definition of ξ_g and ξ_t. Top view of rail elements.

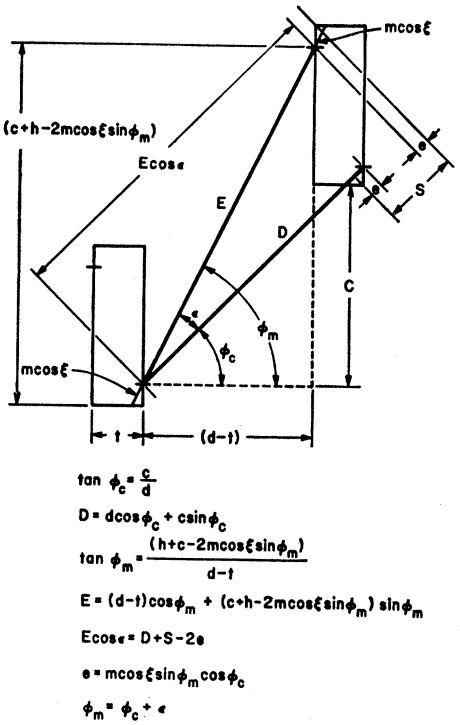

FIG. 13. Definition of ϕ_c. ϕ_m, E, e, ϵ, S and D (end view of rail elements). Note that E and D intercept the detector elements at a distance $m\cos\xi\sin\phi_m$ from the top and bottom of the detector. See Fig. 14.

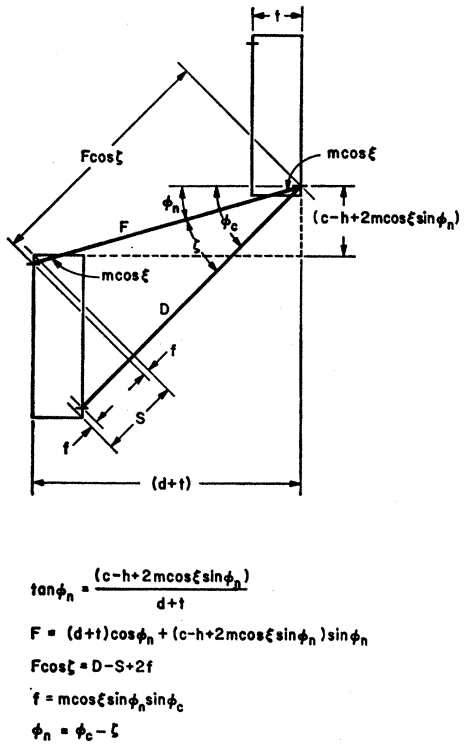

FIG. 14. Definition of ϕ_n, F, f, ζ, and S. (End view of rail elements.) Note that E and D intercept the detector elements at a distance $m\cos\xi\sin\phi_n$ from the top and bottom of the detector.

proach. The total aperture for all pairs in each Class I, II, and III is

$$A_p{}^{\mathrm{I}}=3(8H_p{}^{\mathrm{I}}L_p{}^{\mathrm{I}}), \tag{21}$$

$$A_p{}^{\mathrm{II}}=2(8H_p{}^{\mathrm{II}}L_p{}^{\mathrm{II}}), \tag{22}$$

$$A_p{}^{\mathrm{III}}=1(8H_p{}^{\mathrm{III}}L_p{}^{\mathrm{III}}), \tag{23}$$

where

$$H_p{}^{\mathrm{II}}=H_p{}^{\mathrm{III}}=E(1-\cos\epsilon)+F(1-\cos\zeta)+m[\sin(\epsilon+\phi_c)-\sin\phi_c]^2-m[\sin\phi_c-\sin(\phi_c-\zeta)]^2, \tag{24}$$

$$H_p{}^{\mathrm{I}}=E(1-\cos\epsilon)+m\sin\epsilon, \tag{25}$$

$$L_p{}^{\mathrm{I}}=L_p{}^{\mathrm{II}}=L_p{}^{\mathrm{III}}=\frac{l\pi}{4}-\frac{(d-t)}{\cos\phi_c}-\frac{2m}{3}-G_p(\phi_c), \tag{26}$$

$$G_p=2(Q-1)\left[g\left(\frac{\xi_t}{2}+\frac{\sin2\xi_t}{4}\right)-\left(\frac{t}{\cos\phi_c}\right)\left(\frac{\sin^2\xi_t}{2}\right)+\frac{2m}{3}(1-\cos^3\xi_t)\right]+(Q-1)\left[-g\left(\frac{\xi_g}{2}+\frac{\sin2\xi_g}{4}\right)+\frac{(d+t)\sin^2\xi_g}{2\cos\phi_c}-\frac{2m}{3}(1-\cos^3\xi_g)\right]. \tag{27}$$

The detector dimensions are given in Table VIII. Figures 9 through 14 are useful in visualizing these quantities.